Supplementary Information

Modulating Renal GLUT2 by CB_1 Receptor: Implications for the Treatment of Diabetic Nephropathy

Liad Hinden, Shiran Udi, Adi Drori, Asaad Gammal, Alina Nemirovski, Rivka Hadar, Saja Baraghithy, Anna Permyakova, Matan Geron, Merav Cohen, Sabina Tsytkin-Kirschenzweig, Yael Riahi, Gil Leibowitz, Yaakov Nahmias, Avi Priel, and Joseph Tam

Inventory of Supplemental Information:

The following Supplemental Figures and Experimental Procedures provide an additional information supporting GLUT2 regulation by proximal tubule CB_1R in DN:

Supplementary Figure 1. Experimental design.

Supplementary Figure 2. Peripheral CB_1R blockade reduces diabetes-induced upregulation in Lipocalin 2.

Supplementary Figure 3. GLUT2 antibody specificity.

Supplementary Figure 4. CB_1R regulates perinuclear translocation of GLUT2 in MDCK II cells.

Supplementary Figure 5. Schematic depiction of multicellular cysts formed by MDCK II cells in Matrigel®.

Supplementary Figure 6. Knocking out CB_1R from the RPTCs does not affect GLUT2 expression in the pancreas.

Supplementary Figure 7. Effect of low-dose STZ administration on the kidney and pancreas.

Supplementary Figure 8. Normal urinary levels of kidney injury markers and serum MCP-1 in RPTC-$CB_1R^{-/-}$ mice.

Supplementary Figure 9. Urinary levels of STZ in wild-type and RPTC-$CB_1R^{-/-}$ mice.

Supplementary Figure 10. Effect of administering a high dose of STZ on the pancreas and kidney.

Supplementary Figure 11. SGLT2 expression is not affected by CB_1R genetic deletion or pharmacological blockade.

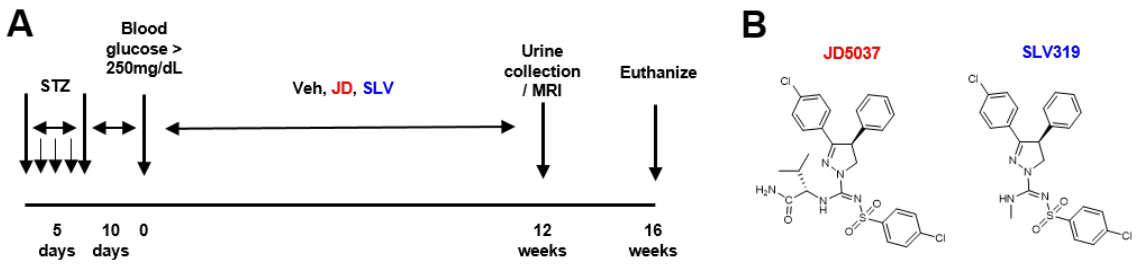

Supplementary Figure 1. Experimental design. Experimental design (see Methods) **(A)**. Structure of JD5037 and its brain-penetrant parent compound, SLV319 **(B)**.

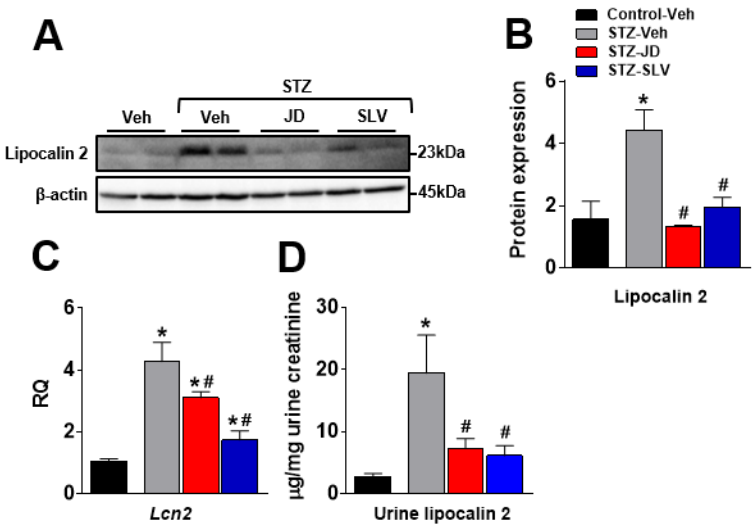

Supplementary Figure 2. Peripheral CB_1R blockade reduces diabetes-induced upregulation in Lipocalin 2. Diabetes-induced upregulation in renal lipocalin 2 protein (**A, B**) and mRNA (**C**) expression levels, as well as its urine excretion rate (**D**) were attenuated/normalized by JD5037 and SLV319 treatment. Data represent the mean±SEM from 8-10 mice per group. *P<0.05 relative to the corresponding control group treated with Veh, #P<0.05 relative to the corresponding STZ group treated with Veh.

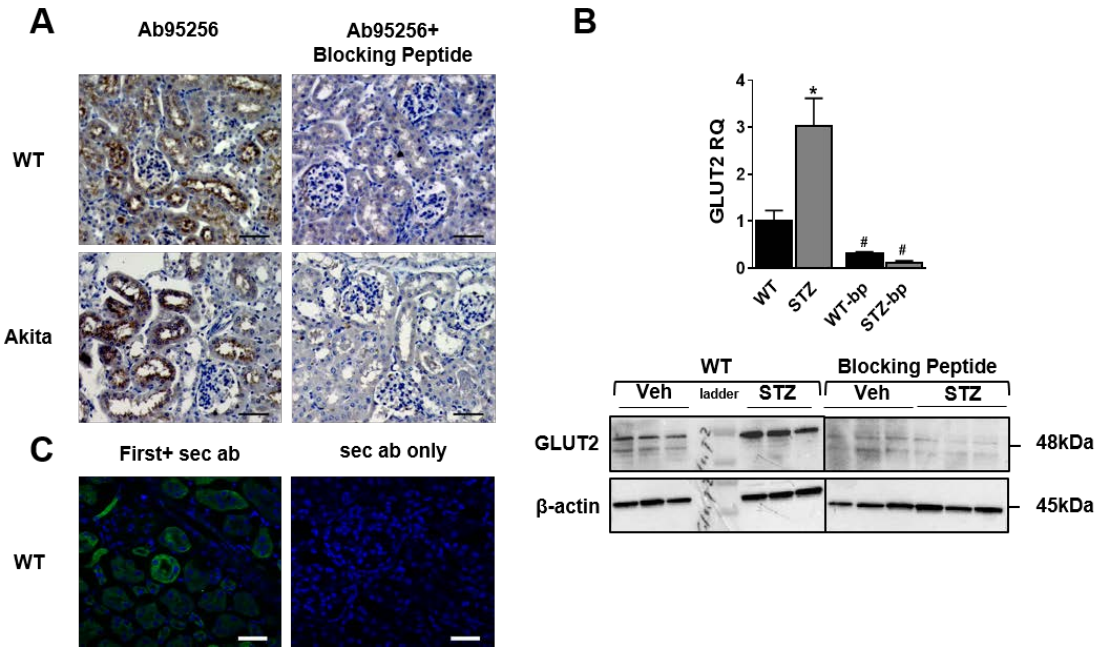

Supplementary Figure 3. GLUT2 antibody specificity. GLUT2 antibody (Abcam, ab95256) specificity was determined by immunohistochemistry (**A**) and Western blotting (**B**) analyses using its blocking peptide (Abcam, ab105630) as well as by immunofluorescence staining (**C**) with/without the secondary antibody (Abcam, ab150077). Data in **A** and **C** are at 40× magnification, scale bar, 50 µm. The data in **B** represent the mean±SEM from 3 mice per group. *P<0.05 relative to WT, $^{\#}$P<0.05 relative to the corresponding WT and STZ without blocking peptide (bp).

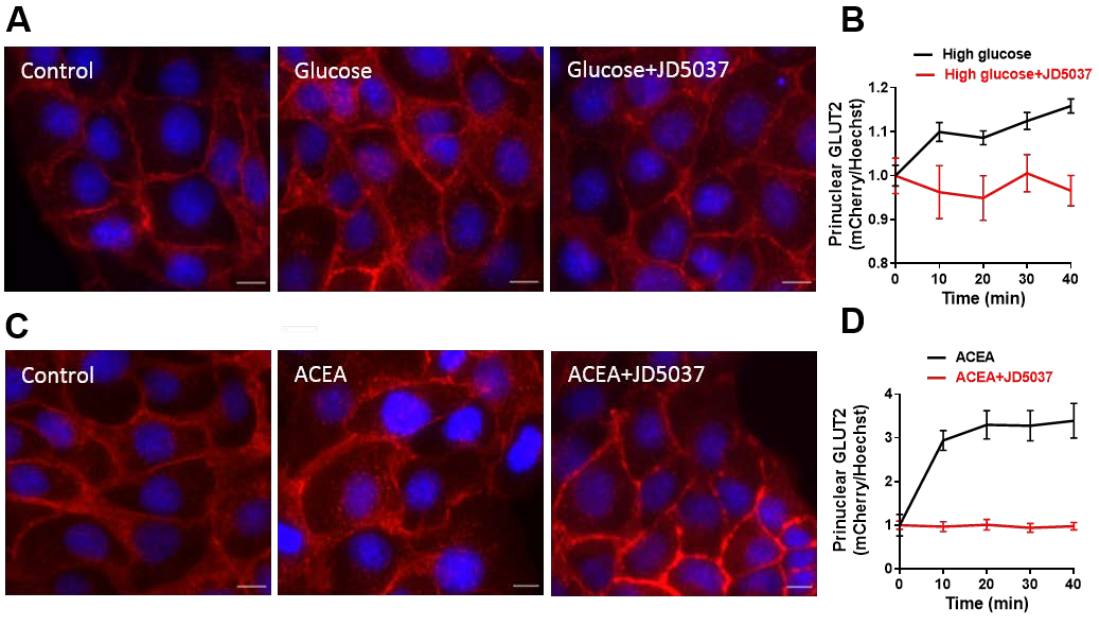

Supplementary Figure 4. CB_1R regulates the perinuclear translocation of GLUT2 in MDCK II cells. High-glucose levels (75 mM) (**A, B**) and stimulating CB_1R by ACEA (10 µM) (**C, D**) resulted in perinuclear translocation of GLUT2 in MDCK II monolayer cells expressing GLUT2–mCherry fusion protein, an effect that was inhibited in the presence of JD5037 (100 nM). Representative pictures from control, high-glucose, and ACEA-treated cells with and without JD5037 (**A, C**) and their corresponding GLUT2 perinuclear measurements (**B, D**), scale bar, 10 µm. Data represent the mean±SEM from 7-10 cells in each frame for each time point.

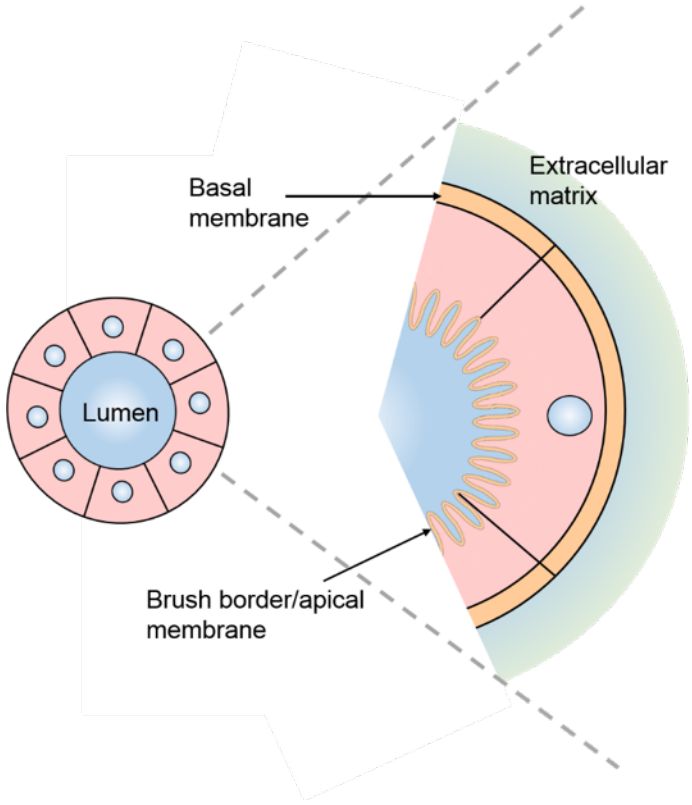

Supplementary Figure 5. Schematic depiction of multicellular cysts formed by MDCK II cells in Matrigel®. Cysts display an internal apical lumen with a brush border membrane and an outer basal surface.

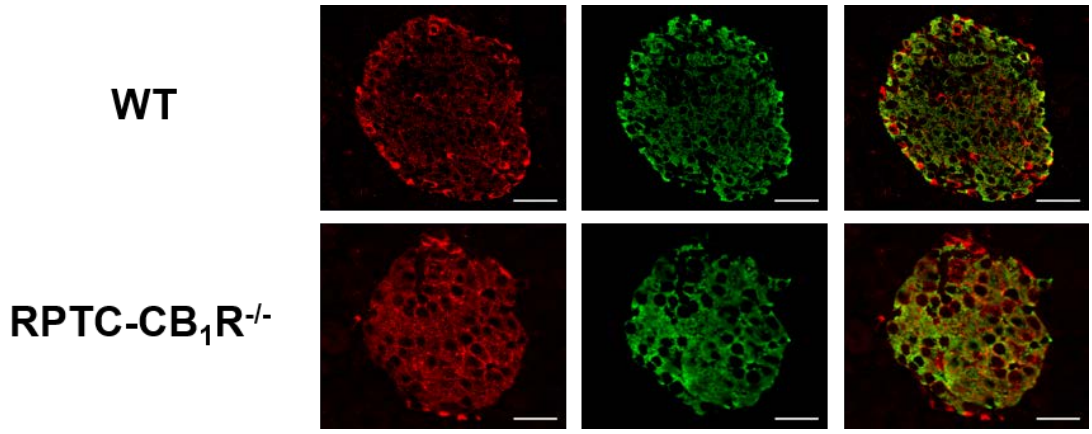

Supplementary Figure 6. Knocking out CB_1R from RPTCs does not affect GLUT2 expression in the pancreas. Representative images of immunostaining for GLUT2 (red) and insulin (green) in pancreatic islets from wild-type and RPTC-$CB_1R^{-/-}$ mice. Scale bars, 25 μm.

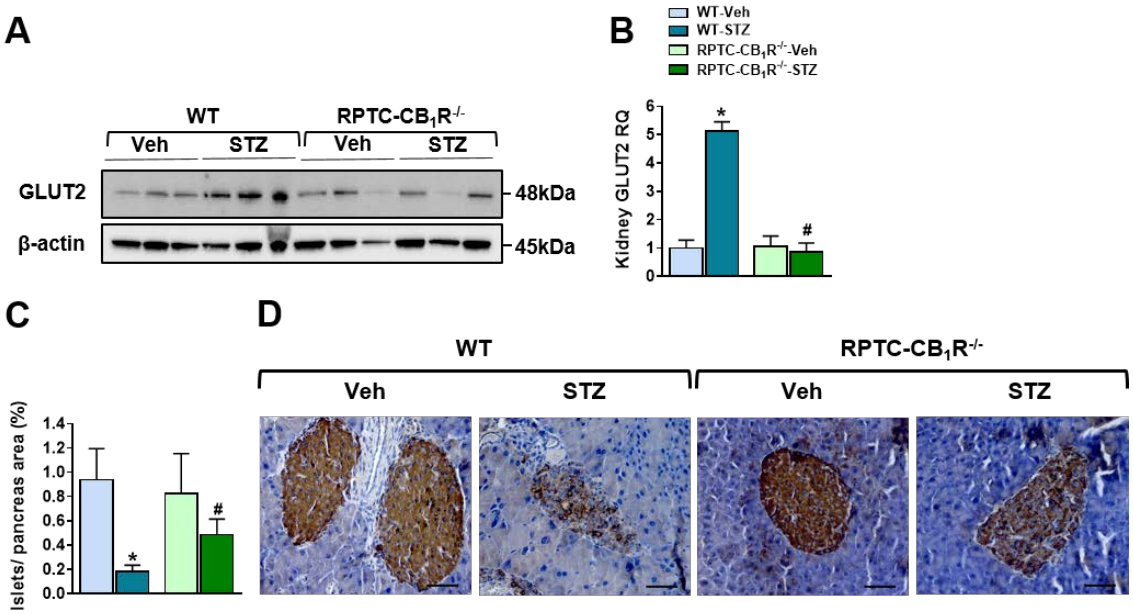

Supplementary Figure 7. Effect of low-dose STZ administration on the kidney and pancreas. Administering a low dose of STZ (50 mg/kg, ip for 5 days) resulted in increased GLUT2 expression in the kidney in wild-type, but not RPTC-$CB_1R^{-/-}$ mice (**A, B**). Preserved islets of Langerhans, as determined by immunohistochemistry for insulin staining, were observed in the STZ-treated RPTC-$CB_1R^{-/-}$ mice (**C, D**). 40× magnification, scale bar, 50 µm. Data represent the mean±SEM from 4-5 mice per group. *P<0.05 relative to animals treated with Veh within the same genotype, $^{\#}$P<0.05 relative to wild-type animals receiving the same treatment.

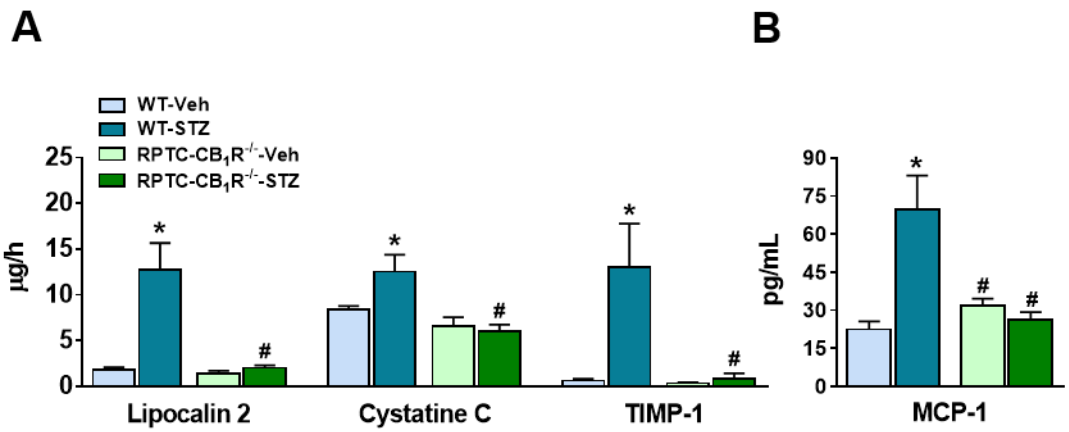

Supplementary Figure 8. Normal urinary levels of kidney injury markers and serum MCP-1 in RPTC-CB$_1$R$^{-/-}$ mice. Diabetes resulted in elevated urinary excretion levels of lipocalin 2, cystatine C, and TIMP-1 (**A**), as well as circulating levels of MCP-1 (**B**). These markers remained normal in RPTC-CB$_1$R$^{-/-}$ mice. Data represent the mean±SEM from 8-10 mice per group. *P<0.05 relative to animals treated with Veh within the same genotype, $^{\#}$P<0.05 relative to wild-type animals receiving the same treatment.

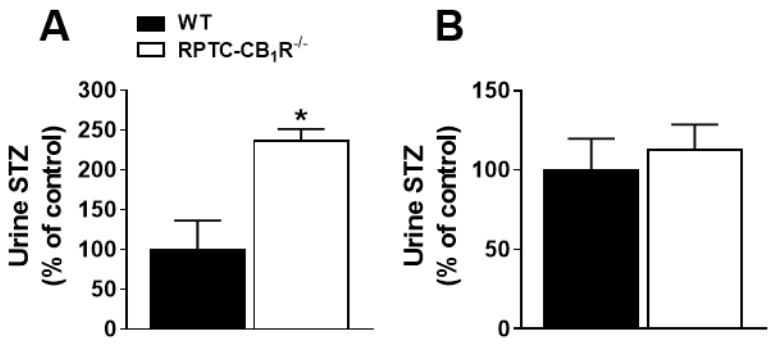

Supplementary Figure 9. Urinary levels of STZ in wild-type and RPTC-$CB_1R^{-/-}$ mice.

Elevated urinary excretion levels (**A**) were found in RPTC-$CB_1R^{-/-}$ mice after administering a low dose (50 mg/kg, ip for 5 days) of STZ, whereas comparable urinary (**B**) levels of STZ in both mouse strains were found following a single high dose of STZ (185 mg/kg, ip). Data represent the mean±SEM from 4-7 mice per group. *P<0.05 relative to wild-type mice.

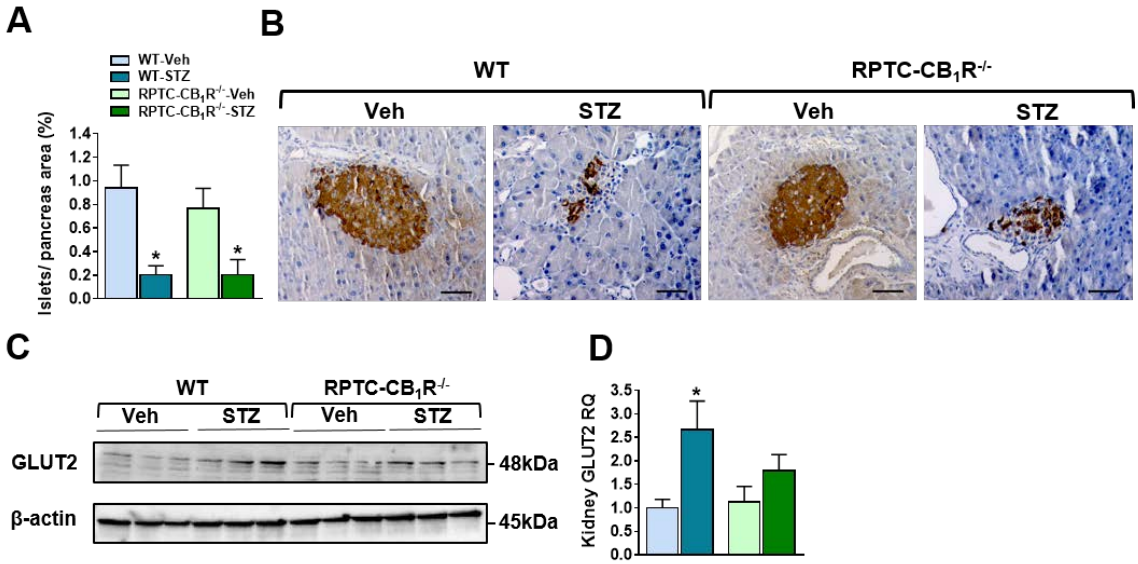

Supplementary Figure 10. Effect of administering a high dose of STZ on the pancreas and kidney. A high single dose of STZ (185 mg/kg, ip) resulted in a comparable reduction in the number of Langerhans islets in both mouse strains (**A, B**), as determined by immunohistochemistry for insulin staining. 40× magnification, scale bar, 50 µm. Increased GLUT2 expression in the kidney was observed in wild-type, but not RPTC-$CB_1R^{-/-}$ mice (**C, D**). Data represent the mean±SEM from 3-4 mice per group. *P<0.05 relative to animals treated with Veh within the same genotype.

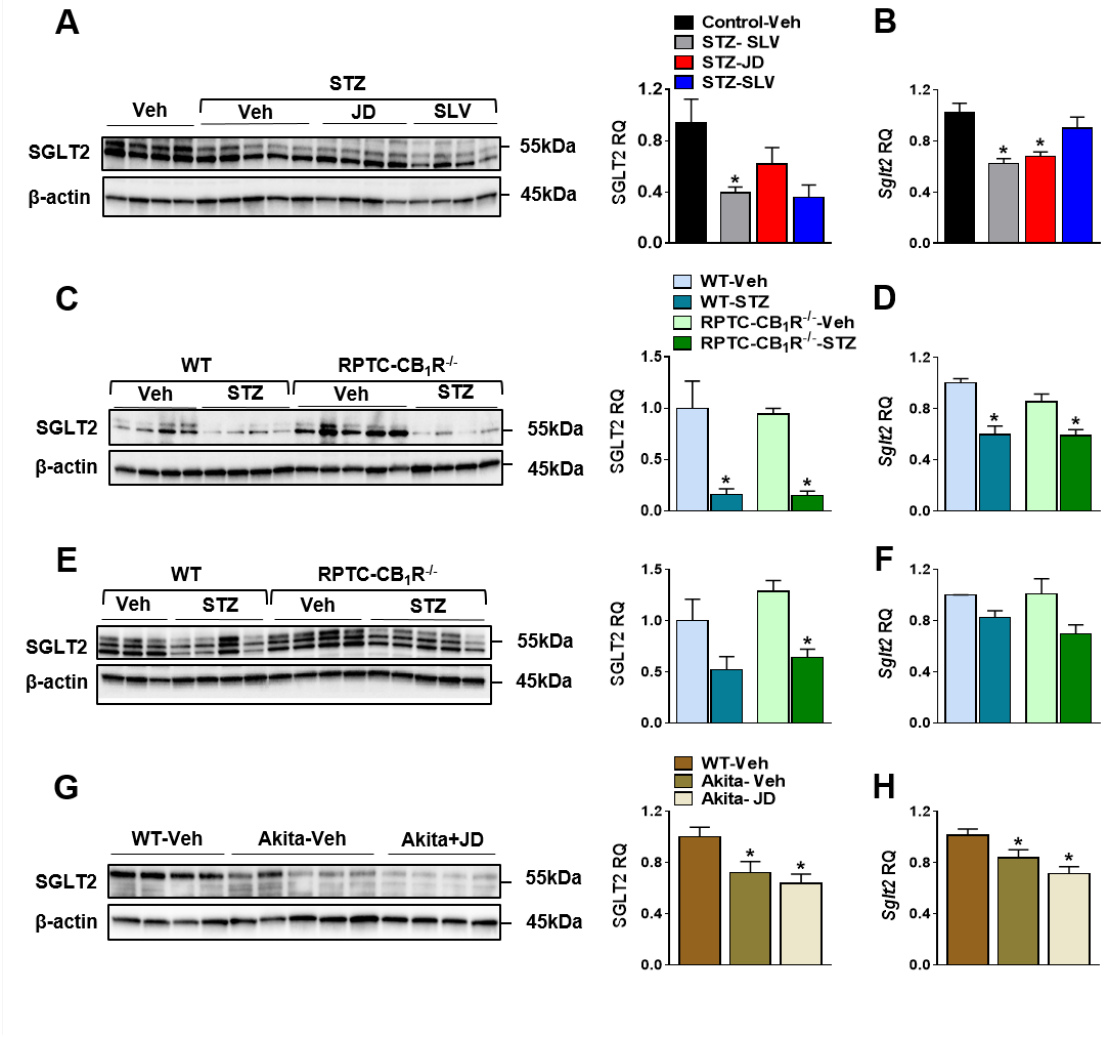

Supplementary Figure 11. SGLT2 expression is not affected by genetic deletion or pharmacological blockade of CB_1R. Protein (**A, C, E, G**) and mRNA (**B, D, F, H**) expression levels of SGLT2, noted in all 4 animal models, were unaffected by genetic deletion (**C-F**) or pharmacological blockade (**A, B, G, H**) of CB_1R. Reduced SGLT2 expression levels were measured under genetic and STZ-induced diabetic conditions (**A-D**). Data represent the mean±SEM from 4-6 mice per group. *P<0.05 relative to animals treated with Veh of the same genotype.

Complete Methods

Animals and experimental protocol. The experimental protocol was approved by the Institutional Animal Care and Use Committee of the Hebrew University of Jerusalem. Male 8-week-old C57Bl/6 mice (Harlan Laboratories) were given five consecutive intraperitoneal STZ injections (Cayman Chemical; 50 mg/kg per day; *'low-dose STZ protocol'*). A control group was given 0.1 mol/L citrate buffer (pH 4.5). STZ-induced diabetic mice were treated daily with SLV319, JD5037 (3 mg/kg, po, each), or a vehicle (Veh; 1% Tween80, 4% DMSO in saline) for 16 weeks, and their controls were given Veh. Body weight and glucose levels were monitored weekly. A similar protocol was implemented in male 8-week-old RPTC-$CB_1R^{-/-}$ mice[1] and their control littermates without administering SLV319 or JD5037. For the *'high-dose STZ protocol'*, 8-week-old male C57Bl/6 or RPTC-$CB_1R^{-/-}$ mice and their control littermates received a single injection of STZ (185 mg/kg, ip), and their body weight and glucose levels were monitored daily. In addition, 7-week-old male *Akita Ins2+/C96Y* diabetic mice were treated daily with JD5037 (3 mg/kg, po, each), or a vehicle (Veh; 1% Tween80, 4% DMSO in saline) for 7 weeks, and their nondiabetic control C57Bl/6 littermates were given Veh.

Twenty-four-hour urine and water consumption were measured using the CCS2000 Chiller System (Hatteras Instruments). Body composition was determined by EchoMRI-100H™ (Echo Medical Systems). After euthanasia, trunk blood was collected, and the kidney and pancreas were removed and weighed, and samples were either snap-frozen or fixed in buffered 4% formalin.

Materials. STZ, ACEA, 2-NBDG, and cytochalazin B were purchased from Cayman Chemical. JD5037 and SLV319 were synthesized as described previously,[2] and purchased from Haoyuan Chemexpress Co., Ltd.

Blood and urine biochemistry. Serum insulin and urine albumin were measured by ELISAs (Millipore and Bethyl Laboratories, respectively). Blood urea nitrogen, urine glucose, and creatinine were determined using Cobas C-111 chemistry analyzer (Roche, Switzerland). Urine lipocalin 2, IP-10, cystatin C, and clusterin were determined by panels 1 & 2 Toxicity Multiplex Assays using Luminex MAGPIX (Millipore). Urine levels of KIM-1, TIMP-1, and LCN2 were measured by ELISA kits (KIM-1 & TIMP-1, R&D Systems, MN, USA; LCN2, BOSTER Biological Technology, CA, USA). Results were normalized to the total urine creatinine.

Histopathological Analyses. Paraffin-embedded kidney and pancreas sections (2 and 5 μm, respectively) from each group (5-6 animals per group) were stained with hematoxylin and eosin or Periodic Acid–Schiff (PAS) followed by hematoxylin staining. Kidney images were taken from 10 random 40x fields from each animal. Glomerular and Bowman's space cross-sectional areas were quantified using ZEN BLUE software (Zeiss, Germany). Tubular necrosis and apoptosis were measured by determining the percentage of tubules that exhibited cell necrosis, loss of the brush border, apoptotic bodies, and cast formation by an individual blinded to the treatment. For each kidney, 20 randomly chosen glomeruli were captured with an AxioCam ICc5 color camera mounted on an Axio Scope.A1 light microscope (Zeiss).

Immunohistochemistry. Kidney and pancreas tissues were fixed in buffered 4% formalin for 48 hr and then embedded in paraffin. Sections were deparaffinized and hydrated. Heat-mediated antigen retrieval was performed with 10 mM citrate buffer pH 6.0 (Thermo Scientific, IL, USA). Endogenous peroxide was inhibited by incubating with a freshly prepared 3% H_2O_2 solution in MeOH. Unspecific antigens were blockaded by incubating sections for 1 hr with 2.5% horse serum (VE-S-2000, Vector Laboratories). For assessment of tubule-interstitial injury, inflammation, and fibrosis, 2 µm kidney sections were stained with rabbit anti-mouse antibodies as described in **Supplementary Table 1**, followed by a goat anti-rabbit HRP conjugate (ImmPRESS™, Vector laboratories). Color was developed after an incubation with 3,3'-Diaminobenzidine (DAB) substrate (ImmPACT DAB Peroxidase (HRP) Substrate, SK-4105, Vector Laboratories), followed by hematoxylin counterstaining and mounting (Vecmount H-5000, Vector laboratories). Stained sections were photographed as described above. The positive area was quantified using Image J with a minimum of 5-6 random kidney sections per mouse.

For assessing the number of Langerhans islets and the cellular structure, pancreas sections were stained with guinea pig anti-insulin (A0564, Dako) antibody, followed by biotinylated secondary antibody and VECTASTAIN ABC reagent (VECTASTAIN ABC-Peroxidase Kit, Vector laboratories). Color was developed after an incubation with 3,3'-Diaminobenzidine (DAB) substrate (ImmPACT DAB Peroxidase (HRP) Substrate, SK-4105, Vector Laboratories), followed by hematoxylin counterstaining and mounting (Vecmount H-5000, Vector laboratories). Stained sections were photographed as described above. Panoramic images were taken for the entire section using ZEN BLUE software (Zeiss, Germany) and the islets-to-pancreas ratio was calculated.

Fluorescence immunohistochemistry. GLUT2 expression in the pancreas was assessed in paraffin-embedded sections that were deparaffinized and underwent antigen retrieval as described above. The sections were co-stained with guinea pig anti-insulin (A0564, Dako), and rabbit anti-GLUT2 (ab95256, Abcam) antibodies, followed by an incubation with donkey anti-guinea pig-AF488 (706545148, Jackson) and donkey-anti-rabbit-APC (711136152, Jackson), respectively. GLUT2 expression in the kidney was assessed in frozen sections. Mice, injected with a single high dose of STZ (185 mg/kg, ip), were treated daily with JD5037 (3 mg/kg, po,) or a vehicle (Veh; 1% Tween80, 4% DMSO in saline) for 1 week. At the end of the treatment, mice were starved overnight, anaesthetized, and their kidneys collected as described previously by Marks and colleagues.[3] Crayo-sections were stained for GLUT2 antibody followed by incubation with gout anti-rabbit-AF488 (ab150077, Abcam). GLUT2 antibody specificity was verified using a blocking peptide or a secondary antibody only (**Supplementary Figure 3**). Sections were mounted with mounting medium with DAPI (H-1200, Vector) and photographed using the LSM 700 imaging system (Zeiss).

Western Blotting. Kidney homogenates were prepared in a RIPA buffer (25mM Tris-HCl pH 7.6, 150 mM NaCl, 1% NP-40, 1% sodium deoxycholate, 0.1% SDS) using BulletBlender® and zirconium oxide beads (Next Advanced, Inc., NY, USA). Protein concentrations were measured with the Pierce™ BCA Protein Assay Kit (Thermo Scientific, IL, USA). Samples were resolved by SDS-PAGE (4-15% acrylamide, 150V) and transferred to PVDF membranes using the Trans-Blot® Turbo™ Transfer System (Bio-Rad, CA). Membranes were then incubated for 1 hr in 5% milk (in 1x TBS-T) to block unspecific binding. Membranes were incubated overnight with rabbit anti-mouse lipocalin

2 (ab70287, Abcam), GLUT2 (ab95256, Abcam), and PKC-β1 (ab195039, Abcam) antibodies at 4°C. GLUT2 antibody specificity was assessed by using its blocking peptide (ab105630, Abcam) at a ratio of 1:10 (**Supplementary Figure 3**). Anti-rabbit horseradish peroxidase (HRP)-conjugated secondary antibodies were used for 1 hr at room temperature and followed by chemiluminescence detection using Clarity™ Western ECL Blotting Substrate (Bio-Rad, CA). Densitometry was quantified using Bio-Rad CFX Manager software. Quantification was normalized to anti-β actin antibody (ab49900, Abcam).

Real-time PCR. Total renal mRNA was extracted and gene expression assays were assessed as described previously[4] using CFX connect™ (Bio-Rad). The following mouse genes were evaluated: *Lcn2, Cst3, Clu, Kim1, Col1a1, Col3a1, Fn1, Timp-1, Tnfα, Il-18, Mgll, Fahh, Ip-10, Mcp-1, Glut2, Sglt2,* and *Cnr1*. All genes were normalized to *Mus musculus Ubc*. The following human genes were evaluated: *TNFα, IL-18, GLUT2, SGLT2,* and *CNR1*. All genes were normalized to human *RPLP0.* (Primer information is described in **Supplementary Tables 2 and 3**).

Cell culture. hRPTCs and DhRPTCs (Lonza) were cultured in REGM BulletKit medium (Lonza), as described previously.[5] MDCK II cells (ATCC) expressing the C-terminal GLUT2–mCherry fusion protein were cultured as described previously.[6]

Calcium imaging. hRPTCs and DhRPTCs were spotted at Poly-D-Lysine (PDL, 0.2 mg/ml) coated imaging chambers (μ-slide, 8 well, ibidi, Germany) 3-4 hr before being loaded with Fura-2AM (Invitrogen, MA, USA; 10 μM) dissolved in ringer's salt solution (in mM: 140 NaCl, 2.5 KCl, 1.8 $CaCl_2$, 2 $MgSO_4$, 20 HEPES and 5 D-glucose, pH 7.4 with NaOH) for 1 hr. Cells were then washed twice with ringer solution and incubated in the

presence/ absence of 100 nM JD5037 for 30 min. Stock solutions of 1M Glucose and 27.3 mM ACEA were dissolved in ringer's solution to obtain the desired concentrations. Using an inverted microscope (Olympus IX70, Japan), cells were illuminated with a xenon arc lamp, and excitation wavelengths (340/380 nm) were selected by using a Lambda DG-4 monochromatic wavelength changer (Sutter Instrument, CA, USA). Fluorescence emission at >480 nm was captured with a front-illuminated interline CCD camera (Exi Blue, QImaging, BC, Canada) and MetaFluor Fluorescence Imaging Software (Universal Imaging Corp., USA), which was also used for offline analysis. Background-corrected 340/380 ratio images were collected every 4 sec.

Small interfering RNA treatment. Small interfering RNA (siRNA) transfection against *Glut2* (sc-35495, Santa Cruz) was performed in hRPTCs using the siRNA reagent system (sc-45064, Santa Cruz) according to the manufacturer's instructions.

2-NBDG assay and flow cytometry. All flow cytometry experiments were conducted in choline chloride Na^+-free buffer (CCB), which contains 140 mM choline chloride, 5 mM KCl, 2.5 mM $CaCl_2$, 1 mM $MgSO_4$, 1 mM KH_2PO_4, 10 mM HEPES (pH 7.4), and 0.1% BSA. hRPTCs were seeded in 12-well plates with REGM BulletKit medium for 24 hr. Then, the medium was replaced with normal medium supplemented with or without 100 nM JD5037 for 30 min or 10 μM cytochalazin B for 10 min. After having been washed, the cells were incubated for 2 hr in the presence or absence of 100 μM 2-NBDG dissolved in CCB with or without high glucose (30 mM) or 10 μM ACEA. GLUT2 expression in hRPTCs and DhRPTCs was analyzed in cells that underwent the 2-NBDG assay, by incubating them with rabbit anti-GLUT2-AF647 antibody (Bioss). Fluorescence was

measured at excitation and emission wavelengths of 485 nm and 528 nm, respectively. The relative florescence intensity (RFI) was used to express fluorescence. For each measurement, data from 5000 single cell events were collected using a CytoFLEX (Beckman Coulter) flow cytometer.

XTT test. hRPTCs were seeded in 96-well plates with REGM BulletKit medium for 24 hr. Then, the medium was replaced with normal glucose medium (5.5 mM) or high glucose medium (30 mM) supplemented with or without 100 nM JD5037 for 1 hr, following by the addition of 10 μM ACEA for 30 hr. The XTT cell viability test was performed following the supplier's instructions (Biological Industries) in six independent experiments.

GLUT2 translocation in MDCK II cells. Monolayer and differentiated hollow polarized cyst cultures of MDCK II cells expressing C-terminal GLUT2–mCherry fusion protein were established as described previously[6]. Monolayer and polarized MDCK II cysts were incubated in PBS with Mg^{2+} and Ca^{2+} (buffer), in the presence or absence of 75 mM glucose, 10 μM ACEA, or 100 nM JD5037. Time-lapse microscopy of GLUT2 translocation was carried out by replacing PBS buffer with one containing 75 mM glucose/10 μM ACEA or vice versa. Inhibition of GLUT2 translocation was carried out by 30 min pre-incubation with 100 nM JD5037. Cells were counterstained with Hoechst for 30 min before visualization. Fluorescence images were taken using a Zeiss LSM 700 imaging system (Carl Zeiss, Germany) equipped with a LD Plan Neufluor 20 objective (NA 0.4, WD 7.9 mm). Images were analyzed using ZEN 2012 BLUE software (Carl Zeiss). Confocal imaging of three-dimensional imaging of spheroids was carried out on the same system in confocal mode using solid-state laser lines 405, 488, 555, and 639 nm.

Confocal images were taken with a C-Apochromat 40x water immersion objective (NA 1.8, WD 0.28 mm). Analysis was carried out using ZEN 2011 BLACK software (Carl Zeiss).

STZ measurements by LC-MS/MS. STZ was detected by a TSQ Quantum Access Max mass spectrometer. The triple quadrupole mass spectrometer was operated in positive ionization mode using electrospray ionization (ESI) and detection and quantification were performed using multiple reaction monitoring (MRM). The high-purity nitrogen gas (15 L min-1), used as sheath and auxiliary gases, was generated using a Parker nitrogen generator (Parker Hannifin ltd., Gateshead, Tyne and Wear, England). 99.999% pure argon (Moshalion, Jerusalem, Israel) was used as collision gas (1.5 mTorr). The spray voltage, sheath and auxiliary gas were set at 4500V, 45 and 25 (arbitrary units), respectively. The skimmer offset, and capillary transfer tube temperature were set at -8V, and 200°C, respectively. The vaporizer temperature within the ESI source was 500°C. The scan time was 100 ms, scan width 0.1 m/z, Q1 and Q3 peak width of 0.7 Da (unit). TSQ Tune Software (Thermo Scientific, San Jose, CA, USA) was used for the optimization of tuning parameters. Data acquisition and processing were carried out using the Xcalibur program (Thermo Scientific, San Jose, CA, USA). The molecular ion of STZ (m/z 266) was selected in the first mass analyzer and fragmented in the collision cell followed by detection of the products of fragmentation in the second analyzer. Two transitions were monitored: m/z 266 → 248 (quantifier), collision energy (CE) 6V and m/z 266 → 111 (qualifier), CE 31V.The chromatography was performed under reverse phase conditions using a Thermo Scientific system (San Jose, CA, USA) which included a Dionex Pump and an Accela Autosampler. The chromatographic separations were performed on a Kinetex™

(Phenomenex, Torrance, CA, USA) column (C8, 2.6 µm particle size, 100 Å pore size, 100 x 2.1 mm), protected by a SecurityGuard™ (Phenomenex, Torrance, CA, USA) ULTRA cartridges (C8, 2 x 2.1 mm). The injection volume was 5 µL, the oven temperature was maintained at 40°C. Isocratic elution mobile phase consisted of 20mM NH_4OAc and 0.2% Acetic Acid in water at 200 µL/min for 3 min. Urine samples underwent a 1:5 dilution using mobile phase prior to analysis.

Statistics. Values are expressed as mean±SEM. Unpaired two-tailed Student's *t*-test was used to determine differences between groups. Results in multiple groups and time-dependent variables were compared by ANOVA followed by a Bonferroni test (GraphPad Prism v6 for Windows). Significance was set at $P < 0.05$.

Supplementary Table 1. List of antibodies used for immunohistochemistry, fluorescence staining and immunoblotting.

Protein	Reference	Supplier
Clusterin	12289-1-AP	Proteintech, USA
Cystatin C	ab109508	Abcam, USA
TNFα	ab6671	Abcam, USA
IP-10	ab9807	Abcam, USA
Collagen-1	ab34710	Abcam, USA
Collagen-3	ab7778	Abcam, USA
TIMP1	10753-1-AP	Proteintech, USA
Fibronectin-1	ab23750	Abcam, USA
GLUT2	ab95256	Abcam, USA
GLUT2 blocking peptide	ab105630	Abcam, USA
Insulin	A0564	Dako, USA
Lipocalin 2	ab70287	Abcam, USA
SGLT2	ab85626	Abcam, USA
PKC-β1	ab195039	Abcam, USA
Donkey anti-guinea pig-AF488	706545148	Jackson, USA
Donkey-anti-rabbit-APC	711136152	Jackson, USA
β-actin	ab49900	Abcam, USA
Gout anti rabbit-AF488	ab150077	Abcam, USA

Supplementary Table 2. Primer information.

Gene	Forward	Reverse
mus musculus Cnr1	AAGTCGATCTTAGACGGCCTT	TCCTAATTTGGATGCCATGTCTC
mus musculus Fn1	ATGTGGACCCCTCCTGATAGT	GCCCAGTGATTTCAGCAAAGG
mus musculus Mgll	ACCATGCTGTGATGCTCTCTG	CAAACGCCTCGGGGATAACC
mus musculus Faah	GTATCGCCAGTCCGTCATTG	GCCTATACCCTTTTTCATGCCC
mus musculus Ip-10	GGATGGCTGTCCTAGCTCTG	TGAGCTAGGGAGGACAAGGA
mus musculus Mcp1	GCATTAGCTTCAGATTTA	TTAAAAACCTGGATCGGAACCAA
mus musculus Glut2	TCAGAAGACAAGATCACCGGA	GCTGGTGTGACTGTAAGTGGG
mus musculus Sglt2	ATGCGCTCTTCGTGGTGCTG	ACCAAAGCGCTTGCGGAGGT
mus musculus Ubc	CAGCCGTATATCTTCCCAGAC	CTCAGAGGGATGCCAGTAATC
homo sapience GLUT2	TGGGCTGAGGAAGAGACTGT	AGAGACTGAAGGATGGCTCG
homo sapience RPLP0	CCAACTACTTCCTTAAGATCATCCAA	ACATGCGGATCTGCTGCTGCA

Supplementary Table 3. Primer information.

Gene	QuantiTect Primer Assays (Qiagen, Germany)
mus musculus Lcn2	QT00113407
mus musculus Cst3	QT00113155
mus musculus Clu	QT00146174
mus musculus Kim1	QT00112427
mus musculus Col1a1	QT00162204
mus musculus Col3a1	QT01055516
mus musculus Timp1	QT00996282
mus musculus Tnfα	QT00104006
mus musculus Il18	QT00171129
homo sapience CNR1	QT02305702
homo sapience TNFα	QT01079561
homo sapience IL18	QT00014560

References

1 Udi S, Hinden L, Earley B, Drori A, Reuveni N, Hadar R, Cinar R, Nemirovski A, Tam J. Proximal tubular cannabinoid-1 receptor regulates obesity-induced CKD. *Journal of the American Society of Nephrology : JASN* 28, 2017

2 Chorvat RJ, Berbaum J, Seriacki K, McElroy JF. JD-5006 and JD-5037: peripherally restricted (PR) cannabinoid-1 receptor blockers related to SLV-319 (Ibipinabant) as metabolic disorder therapeutics devoid of CNS liabilities. *Bioorganic & medicinal chemistry letters* 22:6173-6180, 2012

3 Marks J, Carvou NJ, Debnam ES, Srai SK, Unwin RJ. Diabetes increases facilitative glucose uptake and GLUT2 expression at the rat proximal tubule brush border membrane. *The Journal of physiology* 553:137-145, 2003

4 Knani I, Earley BJ, Udi S, Nemirovski A, Hadar R, Gammal A, Cinar R, Hirsch HJ, Pollak Y, Gross I, Eldar-Geva T, Reyes-Capo DP, Han JC, Haqq AM, Gross-Tsur V, Wevrick R, Tam J. Targeting the endocannabinoid/CB1 receptor system for treating obesity in Prader-Willi syndrome. *Mol Metab* 5:1187-1199, 2016

5 Tam J, Cinar R, Liu J, Godlewski G, Wesley D, Jourdan T, Szanda G, Mukhopadhyay B, Chedester L, Liow JS, Innis RB, Cheng K, Rice KC, Deschamps JR, Chorvat RJ, McElroy JF, Kunos G. Peripheral cannabinoid-1 receptor inverse agonism reduces obesity by reversing leptin resistance. *Cell metabolism* 16:167-179, 2012

6 Cohen M, Kitsberg D, Tsytkin S, Shulman M, Aroeti B, Nahmias Y. Live imaging of GLUT2 glucose-dependent trafficking and its inhibition in polarized epithelial cysts. *Open Biol* 4, 2014